THE JOURNAL OF BIOLOGICAL CHEMISTRY VOL. 290, NO. 45, pp. 26968–26977, November 6, 2015

Mitochondrial Iron-Sulfur Cluster Activity and Cytosolic Iron Regulate Iron Traffic in *Saccharomyces cerevisiae*[*][S]

Received for publication, July 6, 2015, and in revised form, August 17, 2015 Published, JBC Papers in Press, August 25, 2015, DOI 10.1074/jbc.M115.676668

Joshua D. Wofford[‡] **and Paul A. Lindahl**[‡§1]

From the Departments of [‡]*Chemistry and* [§]*Biochemistry and Biophysics, Texas A & M University, College Station, Texas 77843*

Background: A mathematical model of iron trafficking and regulation in yeast cells was developed.
Results: The model simulated experimental data from the literature fairly well.
Conclusion: Both cytosolic iron and an exported product of mitochondrial iron-sulfur cluster activity appear to regulate iron traffic.
Significance: The model has some predictive power that can be used to probe the mechanism of mitochondrial iron diseases.

An ordinary differential equation-based mathematical model was developed to describe trafficking and regulation of iron in growing fermenting budding yeast. Accordingly, environmental iron enters the cytosol and moves into mitochondria and vacuoles. Dilution caused by increasing cell volume is included. Four sites are regulated, including those in which iron is imported into the cytosol, mitochondria, and vacuoles, and the site at which vacuolar Fe^{II} is oxidized to Fe^{III}. The objective of this study was to determine whether cytosolic iron (Fe_{cyt}) and/or a putative sulfur-based product of iron-sulfur cluster (ISC) activity was/were being sensed in regulation. The model assumes that the matrix of healthy mitochondria is anaerobic, and that in ISC mutants, O_2 diffuses into the matrix where it reacts with nonheme high spin Fe^{II} ions, oxidizing them to nanoparticles and generating reactive oxygen species. This reactivity causes a further decline in ISC/heme biosynthesis, which ultimately gives rise to the diseased state. The ordinary differential equations that define this model were numerically integrated, and concentrations of each component were plotted *versus* the concentration of iron in the growth medium and *versus* the rate of ISC/heme biosynthesis. Model parameters were optimized by fitting simulations to literature data. The model variant that assumed that both Fe_{cyt} and ISC biosynthesis activity were sensed in regulation mimicked observed behavior best. Such "dual sensing" probably arises in real cells because regulation involves assembly of an ISC on a cytosolic protein using Fe_{cyt} and a sulfur species generated in mitochondria during ISC biosynthesis and exported into the cytosol.

Iron is a critical component of virtually all living systems; it participates in enzyme catalysis, electron-transfer reactions, substrate binding, DNA replication and repair, and many other types of reactions. In eukaryotic cells, iron-rich respiratory complexes in mitochondria are filled with hemes and iron-sulfur clusters (ISCs).[2] Environmental iron is imported into cells where it is trafficked to various cellular compartments. How this traffic is regulated remains an enigma despite extensive investigations (1). Here, we use mathematical modeling to better understand iron regulation in yeast cells.

Environmental iron is generally present as poorly soluble Fe^{III} that is reduced to Fe^{II} before it enters the cell (2). Iron enters through various importers, including a high affinity importer consisting of a permease (Ftr1) and a multicopper oxidase (Fet3). Imported iron is released into the cytosol, probably in the Fe^{II} state. Little is known about cytosolic iron (Fe_{cyt}) because no trafficking species has been isolated or characterized. This is unfortunate because Fe_{cyt} plays an essential role in iron trafficking, and it cannot be ignored in developing a mathematical model of iron trafficking and regulation.

Kaplan and co-workers (3, 4) have indirectly monitored the concentration of Fe_{cyt} by genetically installing iron-requiring enzymes into *Saccharomyces cerevisiae*. In iron-deficient cells, the heterologously expressed enzymes are inactive because they lack iron at their active sites. The enzymes develop activity in cells grown on medium containing iron (Fe_{med}) at high concentrations. These reporter proteins develop activity at rates and to extents that are proportional to $[Fe_{med}]$. These and other experiments suggest that in WT cells, $[Fe_{cyt}]$ qualitatively mirrors the concentration of $[Fe_{med}]$. We will assume this here, but not that $[Fe_{med}]$ and $[Fe_{cyt}]$ are *directly* proportional; $[Fe_{cyt}]$ is expected to be tightly regulated such that it changes modestly as $[Fe_{med}]$ changes dramatically.

Mitochondria are the major iron traffic hubs in eukaryotes. The organelle from *respiring* yeast cells grown in iron-sufficient medium contains 500 – 800 μM iron, most of which is present as Fe_4S_4 clusters and heme centers housed in respiration-related proteins (5). $[Fe_2S_2]^{1+/2+}$ clusters and Fe^{III} phosphate oxyhydroxide nanoparticles are also present. Mitochondria from iron-sufficient *fermenting* cells contain iron at a similar concentration but in a different distribution; the concentration of iron

* This work was supported, in whole or in part, by National Institutes of Health Grant GM084266. This work was also supported by Robert A. Welch Foundation Grant A1170. The authors declare that they have no conflicts of interest with the contents of this article.
[S] This article contains supplemental data A and B and Tables S1–S3.
[1] To whom correspondence should be addressed: Dept. of Chemistry, Texas A & M University, College Station, TX 77843-3255. Tel.: 979-845-0956; Fax: 979-845-4719; E-mail: lindahl@chem.tamu.edu.

[2] The abbreviations used are: ISC, iron-sulfur cluster; Fe_{cyt} or C, cytosolic iron; NHHS, nonheme high spin; F2, NHHS Fe^{II} ions in vacuoles; F3, NHHS Fe^{III} ions in vacuoles; FM, NHHS Fe^{II} ions in mitochondria; FS, $[Fe_4S_4]^{2+}$ clusters and low spin Fe^{II} hemes in mitochondria; MP, mitochondrial nanoparticles; N, nutrient iron added to the growth medium; ROS, reactive oxygen species; VP, vacuolar nanoparticles.

associated with respiratory complexes is reduced ~3-fold (implying a decline from ~600 to 200 μM in iron). In contrast, the concentrations of nonheme high spin (NHHS) Fe^{II} ions, NHHS Fe^{III} ions, and Fe^{III} phosphate oxyhydroxide nanoparticles are increased to ~130, 100, and 200 μM, respectively. These latter three pools are probably related through redox and ligand exchange reactions.

Vacuoles are another iron traffic hub in yeast. These acidic organelles dynamically store and mobilize iron. They are devoid of iron under iron-deficient conditions. Vacuoles from cells grown on iron-sufficient medium contain high concentrations of a NHHS Fe^{III} complex in which the coordinating ligands are closely related to polyphosphate (6). A NHHS Fe^{II} species evident in Mössbauer spectra of adenine-deficient whole cells may also be located in vacuoles (7). Under adenine-sufficient conditions in which the vacuolar iron importer Ccc1 is either absent or overproduced, high levels of Fe^{II} are present (6).

Mössbauer spectra of whole yeast cells exhibit major contributions from both traffic hubs (8). In iron-sufficient WT cells, vacuolar iron exhibits a sextet that accounts for ~70% of spectral intensity. Much of the remaining intensity arises from mitochondrial iron, including a central quadrupole doublet that arises from $[Fe_4S_4]^{2+}$ clusters and low spin Fe^{II} hemes and quadrupole doublets that arise from high spin Fe^{II} heme and NHHS Fe^{II} ions. The intensity of the NHHS Fe^{II} doublet in whole cell spectra is greater than can be accounted for by Fe^{II} ions in mitochondria alone; Fe^{II}_{cyt} and vacuolar Fe^{II} ions probably also contribute.

We define *iron-deficient* conditions as minimal medium supplemented with bathophenanthroline disulfonate and 1 μM $^{57}Fe^{III}$ citrate. We define *iron-sufficient* conditions as the same medium supplemented with 10–40 μM $^{57}Fe^{III}$ citrate, and *iron excess* conditions as the medium supplemented with ≥100 μM $^{57}Fe^{III}$ citrate. Other researchers might use different media and supplement with Fe^{II} rather than Fe^{III} ions, making quantitative comparisons difficult.

In our studies, the overall concentration of iron in cells grown on iron-deficient, iron-sufficient, and iron excess conditions is ~ 200, 400, and 600 μM iron, respectively. Iron-deficient cells are largely devoid of vacuolar iron; their Mössbauer spectra are dominated by the central doublet and an unusually strong NHHS Fe^{II} doublet (5). Mitochondria isolated from iron-deficient cells contain less iron than do mitochondria from iron-sufficient or iron-excess ones (~400 μM *versus* 700–800 μM), but they contain similar levels of respiration-related ISCs and heme centers. This has ramifications for the mechanism of iron regulation.

Fe_{cyt} is trafficked into the mitochondria via two paralogous inner membrane transporters, namely Mrs3 and Mrs4 (Mrs3/4) (9, 10). Imported mitochondrial NHHS Fe^{II} ions are primarily used for heme and ISC biosynthesis. At higher $[Fe_{med}]$, Fe_{cyt} is also trafficked into vacuoles through the Ccc1 importer (11, 12). These are the major iron traffic patterns in a yeast cell (Fig. 1). There are other secondary import and trafficking pathways but they will be ignored here.

The best studied mechanism of iron regulation in *S. cerevisiae* involves Aft1 and Aft2 (13–16). These transcriptional activators control expression of 20–30 genes known as the "iron regulon," including, but not limited to genes *FET3*, *FTR1*, *FET5*, *FTH1*, *SMF3*, *ISU1*, *GRX4*, *MRS4*, and *CTH2*. Aft1 and Aft2 have slightly different functions (13, 17), but these differences will be ignored here. In iron-deficient cells, Aft1/2 monomers are located in the nucleus (18) where they are bound to promotor sites and serve to activate the iron regulon. Under iron-sufficient and iron-excess conditions, Aft1/2 release from these sites, exit the nucleus, and dimerize, thereby deactivating the iron regulon. Aft1/2 dimers bind a Fe_2S_2 cluster that bridges the two subunits (19). These events are part of a signal transduction regulatory pathway that originates in mitochondria (Fig. 2).

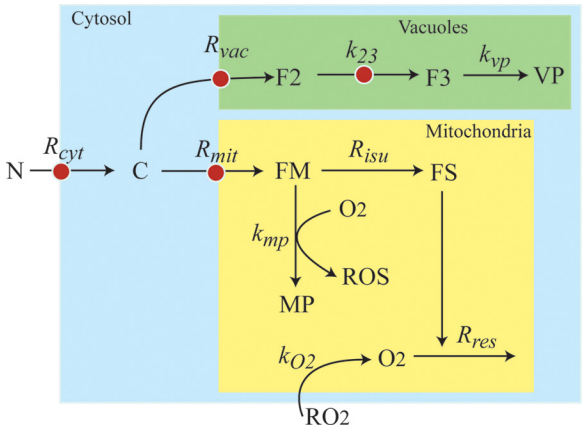

FIGURE 1. **Chemical model of iron trafficking and regulation in *S. cerevisiae*.** Nutrient Fe^{III} citrate (N) becomes cytosolic Fe^{II} (C) as it enters the cell. C moves into the vacuole forming F2 (Fe^{II}), which oxidizes to Fe^{III} (F3) and converts into nanoparticles (VP). C also moves into mitochondria, forming FM (Fe^{II}), which is used to generate FS. This component symbolizes ISCs and heme centers. FS is inserted into respiratory complexes, which function to maintain an O_2-free environment in healthy mitochondria. Some O_2 that diffuses into the matrix reacts with FM to generate mitochondrial nanoparticles and ROS. *Red dots* indicate the four regulated sites.

The form of iron sensed by Aft1/2 has been considered since the mid 1990s, when Yamaguchi-Iwai *et al.* (13, 14) monitored Aft1 activity using Fet3 expression as a reporter. Fet3 expression increases under iron-deficient conditions relative to iron-sufficient ones (supplemental Table S1 and Ref. 46). The Aft1/2-dependent regulatory system was initially assumed to sense Fe_{cyt} (11–14), but the situation changed starting in circa 2004 when Kaplan, Winge, and co-workers (3) determined that Aft1/2-dependent iron regulation was sensitive to ISC biosynthesis in the matrix of mitochondria rather than to Fe_{cyt}.

Deleting proteins that are involved in mitochondrial ISC biosynthesis, such as Yfh1, Atm1, and Yah1, affords an unusual phenotype that has been characterized extensively and has been used to probe the mechanism of Aft1/2-based regulation (20–22). The so-called *ISC mutant phenotype* includes the (*a*) increase of cytosolic and mitochondrial iron import rates, (*b*) accumulation of Fe^{III} phosphate oxyhydroxide nanoparticles in mitochondria, (*c*) decline of both ISCs and hemes in mitochondria, (*d*) increase of ROS damage in mitochondria, (*e*) absence of vacuolar iron in cells grown on iron-sufficient media, and (*f*) increase of cytosolic iron levels.

These effects are absent when ISC mutant cells are grown anaerobically (21, 22). The iron regulon is active in such mutant cells, even when grown on high $[Fe_{med}]$. The discovery that

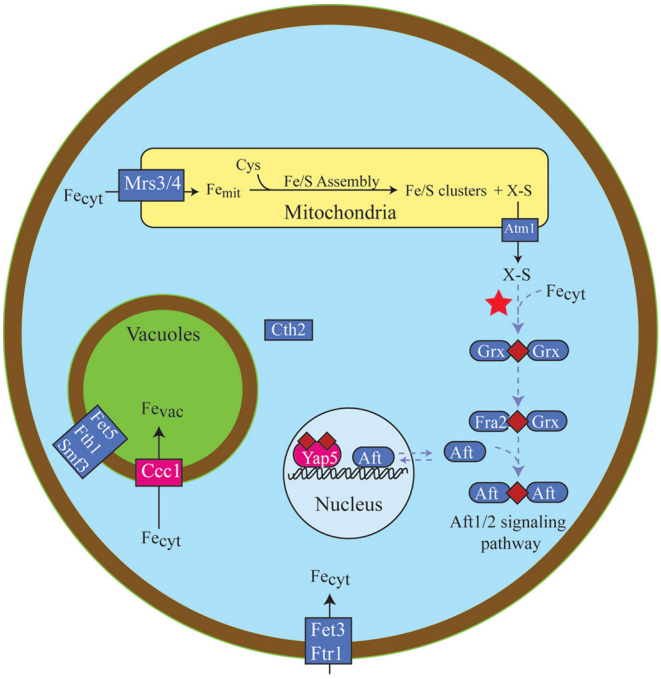

FIGURE 2. **Iron regulation pathways in *S. cerevisiae*.** ISC assembly in mitochondria is thought to generate a sulfur-based species called X-S that is exported from the organelle, possibly through Atm1. X-S and Fe_{cyt} combine in the cytosol to generate a Fe_2S_2 cluster bridged between two glutaredoxin monomers (*red star*). This reaction is proposed to be the origin of Dual regulation. In the Aft1/2 signaling pathway (*purple symbols*) and under iron-sufficient conditions, the cluster is passed to Aft1/2 (via Fra2), which prevents activation of the iron regulon in the nucleus. Under iron-deficient conditions, cluster-free monomeric Aft1/2 activates the iron regulon including the Fet3/Ftr1 importer on the plasma membrane. Cth2, Fet5, and Smf3 are also regulated to control vacuole iron levels. Less is known about Yap signaling pathway (*red symbols*). An ISC is likely built on an unknown protein and transferred eventually to Yap5. Cluster-bound Yap5 activates Ccc1, which imports cytosolic iron into the vacuoles.

[Fe_{cyt}] is not low in ISC mutant cells (23) raised the possibility that Fe_{cyt} may not be sensed in cellular iron regulation.

An elaborate scenario has developed to explain how a signal originating in mitochondria can be relayed to Aft1/2 in the nucleus (Fig. 2). Atm1, an ATP-binding cassette half-transporter on the inner membrane of mitochondria, is thought to export a sulfur-containing by-product of ISC assembly called "X-S" (24, 25). The identity of X-S is unknown, but it is thought to pass through a cavity sized for a small metabolite such as glutathione persulfide (26). X-S provides the sulfur required for cytosolic ISC biosynthesis and indirectly controls Aft1/2 activity and the iron regulon. The sulfur is probably used to build the Fe_2S_2 cluster that bridges a homodimer of Grx3/4 in the cytosol (27). These monothiol glutaredoxins are critical for Aft1/2-dependent regulation. The absence of Grx3/4 activates the iron regulon (28) as this disrupts the signal transduction pathway. Fra2 reacts with the Grx·Fe_2S_2·Grx homodimer to generate a Grx·Fe_2S_2·Fra2 heterodimer (19, 28, 29). This heterodimer donates its Fe_2S_2 cluster to two Aft1/2 monomers to generate the Aft·Fe_2S_2·Aft homodimer, titrating away apo-Aft1/2 monomers that would otherwise bind tightly to iron regulon promotor sites on DNA. In this way, ISC biosynthesis in mitochondria controls the activity of the iron-regulon in the nucleus.

Iron traffic into and out of vacuoles is also highly regulated, with Yap5 playing the dominant role (30). This iron-sensitive transcription factor is constitutively expressed in the nucleus where it is bound to the promoters of *CCC1* (and other genes) to regulate expression (Fig. 2). Earlier studies suggested that Yap5 senses Fe_{cyt} (31), but a later study (4) found that it senses mitochondrial ISC synthesis activity. When ISC synthesis is blocked, Yap5 transcription levels decline, and vacuoles no longer fill with iron (31). However, Yap5 is not controlled by Aft1/2, and the Yap5 signaling pathway does not involve Grx proteins. Yap5 contains seven cysteine residues that are used in iron sensing. Under high iron conditions, Yap5 uses them to bind two Fe_2S_2 clusters (32). This alters the conformation of the protein such that it binds DNA and promotes *CCC1* expression.

Fet5 and Fth1, respective homologs of Fet3 and Ftr1, are also involved in regulating vacuolar iron. The Fet5·Fth1 complex on the vacuolar membrane exports iron to the cytosol. Expression levels of *FET5* and *FTH1* increase under iron-deficient conditions because they are part of the iron regulon (33). *SMF3* is another iron exporter on the vacuolar membrane and is also part of the Aft1/2 system (15). Aft1/2-dependent activation under extreme iron-deficient conditions increases expression of *CTH2* (31). Cth2 binds to and destabilizes *CCC1* mRNA transcripts (34) preventing vacuoles from importing Fe_{cyt}.

Iron traffic into mitochondria is also regulated. Deleting *MRS3/4* affords mitochondria with reduced ISC and heme activities and lower iron concentrations (9, 10). Although the exact species imported by Mrs3/4 is/are unknown, members of this family transport small metabolites and cofactors (35). Δ*MRS3/4* cells acquire more than normal amounts of iron because the Aft1/2-dependent iron regulon is activated due to low ISC activity (9, 10). Mrs4 expression in Δ*YFH1* cells is higher than in WT cells, indicating an up-regulation of mitochondrial iron import under ISC mutant conditions. Activating Aft1/2 under iron-deficient conditions also enhances MRS4 expression (17).

Cells lacking Ccc1 are sensitive to high iron levels in the medium because Fe_{cyt}, which most likely engages in ROS-generating chemistry, is probably present at higher than normal concentrations. Overexpressing Mrs3/4 suppresses that sensitivity probably because it imports more Fe_{cyt} into mitochondria (36). Cells lacking Mrs3/4 up-regulate Ccc1 activity— evidence of what Kaplan calls a "mitochondrial vacuolar" signaling pathway (36).

Materials and Methods

A chemical model was developed to describe trafficking and regulation of iron in yeast cells (Fig. 1); reactions and rate expressions are listed in Table 1. Relevant data were obtained from WT and ISC mutant cells grown in batch culture under iron-deficient, iron-sufficient, and iron excess conditions (supplemental Tables S1 and S2). Cells in these studies were generally harvested during exponential phase.

The concentrations of iron-containing components in exponentially growing cells should be invariant with time. In an expanding steady state, the increase in cellular iron caused by iron influx is counterbalanced by the dilution of cellular iron caused by increasing cell volume. The exponential growth rate of the cell, defined as $\alpha = (1/V) \times (dV/dt)$, is an essential aspect

TABLE 1
Model reactions and rate expressions, including optimized WT parameters

Reactions and Optimized Parameters	Rate Expressions
$\boxed{N \longrightarrow C}$ R_{cyt} = 410 μM·hr^{-1} K_{cyt} = 14 μM $[C]_{spcyt}$ = 27 μM *csencyt* = 5 $[FS]_{spcyt}$ = 190 μM *fssencyt* = 9	$\frac{R_{cyt}\cdot[N]}{K_{cyt}+[N]}\frac{1}{1+\left(\frac{[C]}{[C]_{spcyt}}\right)^{csencyt}}\frac{1}{1+\left(\frac{[FS]}{[FS]_{spcyt}}\right)^{fsencyt}}$
$\boxed{C \longrightarrow FM}$ R_{mit} = 900 μM·hr^{-1} K_{mit} = 12 μM $[C]_{spmit}$ = 80 μM *csenmit* = 5 $[FS]_{spmit}$ = 200 μM *fssenmit* = 4	$\frac{R_{mit}\cdot[C]}{K_{mit}+[C]}\frac{1}{1+\left(\frac{[C]}{[C]_{spmit}}\right)^{csenmit}}\frac{1}{1+\left(\frac{[FS]}{[FS]_{spmit}}\right)^{fsenmit}}$
$\boxed{C \longrightarrow F2}$ R_{vac} = 1500 μM·hr^{-1} K_{vac} = 5.5 μM $[C]_{spvac}$ =1.2 μM *csenvac* = 3 $[FS]_{spvac}$ = 190 μM *fssenvac* = 8	$\frac{R_{vac}\cdot[C]}{K_{vac}+[C]}\left(1-\frac{1}{1+\left(\frac{[C]}{[C]_{spvac}}\right)^{csenvac}}\right)\left(1-\frac{1}{1+\left(\frac{[FS]}{[FS]_{spvac}}\right)^{fsenvac}}\right)$
$\boxed{F2 \longrightarrow F3}$ k_{23} = 7.3 hr^{-1} $[C]_{sp23}$ =2 μM *csen23* = 10 $[FS]_{sp23}$ = 210 μM *Fssen23* = 10	$k_{23}[F2]\left(1-\frac{1}{1+\left(\frac{[C]}{[C]_{sp23}}\right)^{csen23}}\right)\left(1-\frac{1}{1+\left(\frac{[FS]}{[FS]_{sp23}}\right)^{fsen23}}\right)$
$\boxed{FM \longrightarrow FS}$ R_{isu} = 250 μM·hr^{-1} K_{isu} = 610 μM	$\frac{R_{isu}[FM]}{K_{isu}+[FM]}$
$\boxed{O2 \longrightarrow}$ k_{res} = 150 hr^{-1} K_{res} = 9 μM	$\frac{k_{res}[FS][O2]}{K_{res}+[O2]}$
$\boxed{FM+O_2 \longrightarrow MP+ROS}$ k_{mp} = 0.18 μM^{-1}hr^{-1}	$k_{mp}[FM][O2]$
$\boxed{F3 \longrightarrow VP}$ k_{vp} = 0.02 hr^{-1}	$k_{vp}[F3]$
$\boxed{O_{2(cytosol)} \longrightarrow O_{2(matrix)}}$ k_{O2} = 52 hr^{-1} [*RO2*] = 100 μM	$k_{o2}\left([RO2]-[O2]\right)$

of our model. When cells grow exponentially, α is constant which makes it particularly easy to evaluate. Assuming that the optical density of cells is proportional to cell volume, α equals the slope of the straight line that results when the natural logarithm of A_{600} is plotted *versus* time ($\ln OD_t = \ln OD_0 + \alpha t$).

Modeling homeostatic regulatory systems that control cytosolic, mitochondrial, and vacuolar iron import on the molecular level is currently not feasible because many critical details remain unknown. Our goal was merely to explore essential aspects of the regulation at four key traffic sites. To do this, we used surrogate mathematical expressions—called "Reg functions"—to mimic regulatory behavior (6, 37). Reg functions can be viewed as valves that dynamically adjust between closed and fully opened to smoothly regulate traffic flow through a site. These functions are characterized by the iron species that they sense (S), the set point concentration at which the valve is half-opened ($[S]_{sp}$), and the sensitivity of the response (*sen*). There are two types of Reg functions, called Reg_{-S} and Reg_{+S}, defined as follows.

$$Reg_{-s} = \frac{1}{1+\left(\frac{[S]}{[S]_{sp}}\right)^{sen}};\ Reg_{+S} = 1 - Reg_{-S} \qquad \text{(Eq. 1)}$$

When $[S] > [S]_{sp}$, the Reg_{-S} valve closes and cell growth dilutes S toward $[S]_{sp}$. When $[S] < [S]_{sp}$, the Reg_{-S} valve opens to achieve the same effect. Reg_{+S} behaves the same as Reg_{-S} but in the opposite direction (closing the valve when [S] is low and opening it when [S] is high). A Reg_{-S} function should be used when the homeostatic response *opposes* the perturbation. Thus, if the concentration of the sensed species is too high, the response of Reg_{-S} would be to decrease flow. A Reg_{+S} function should be used when the homeostatic response reinforces the perturbation; if the concentration of the sensed species is too high, Reg_{+S} increases the flow.

In addition to including regulation at the site of iron import into the cytosol, and at the two sites through which iron moves into mitochondria and vacuoles, the model includes a fourth regulatory site in which vacuolar Fe^{II} (called F2) is oxidized to Fe^{III} (F3). There are a number of conditions and genetic strains (iron-deficient, adenine-deficient, ΔCCC1, and CCC1 overexpression) in which F3 levels are low and F2 levels are high relative to iron-sufficient adenine-sufficient WT conditions (Refs. 5–7 and supplemental Table S1). The model regulates the rate of this oxidation to recreate the effect.

We wanted to evaluate whether Fe_{cyt} (called C in our model) or mitochondrial ISC activity (proportional to the concentration of FS in our model) was sensed in regulation. To do this, three model variants were considered. The *C-Reg* variant assumes that all four regulatory valves exclusively sense C. For rates associated with importing iron into the cytosol (R_{cyt}) and into mitochondria (R_{mit}), Reg_{-C} functions shut down import when [C] is too high. For rates associated with importing C into vacuoles (R_{vac}) or oxidizing F2 to F3 (R_{23}), Reg_{+C} functions are needed.

The FS-Reg variant exclusively senses the activity of ISC assembly in the mitochondria, which in our model generates FS (a substitute for X-S). Reg_{-FS} functions regulate R_{cyt} and R_{mit}, whereas Reg_{+FS} functions regulate R_{vac} and R_{23}. The Dual-Reg variant assumes that both C and FS are sensed at all four regulation sites. To control the rates of R_{cyt} and R_{mit}, we used the product of two Reg_{-S} functions (see supplemental information for a derivation). A similar $\{Reg_{+C}\cdot Reg_{+FS}\}$ product function was used to control R_{vac} and R_{23}.

Inferring the appropriate Reg functions to describe the regulation of vacuolar iron requires some consideration. At the transcriptional level, *CCC1* expression is regulated by Yap5 activity. The response to high [C] and/or [FS] is to increase flow into vacuoles, implying that Reg_{+C} and Reg_{+FS} functions should be used. At the translational level, Ccc1 mRNA is degraded by Cth2 which is regulated, in turn, by Aft1/2. The cell response to low [C] and/or [FS] is to decrease flow through Ccc1 (via increasing Cth2-associated Ccc1 degradation). This

effect again implies use of Reg_+ functions. Deleting Mrs3/4 causes Ccc1 activity to increase (36); thus Mrs3/4 can be viewed as inhibiting Ccc1—analogous to the overall effect of Cth2—again implying use of Reg_+ functions. Finally, Smf3 and Fet5 export vacuolar iron into the cytosol, and an increase in either protein (which are both controlled by the Aft1/2-dependent iron regulon and thus are up-regulated under iron-deficient conditions) causes loss of vacuolar iron. This has the same net effect as inhibiting *CCC1* expression. In summary, although Yap5, Cth2, Mrs3/4, Smf3, and Fet5 regulate vacuolar iron by different mechanisms, their effects can be collectively simulated using Reg_+ functions.

The model presumes a cell encapsulated by a semipermeable membrane surrounded by an environment containing Fe^{III} citrate (N) and molecular oxygen (RO2). The *in silico* cell is composed exclusively of cytosol, mitochondria, and vacuoles such that $V_{cell} = V_{cyt} + V_{vac} + V_{mit}$. The model involves seven chemical components that contain iron and four that do not (Fig. 1). In addition to F2 and F3, vacuoles contain nanoparticles (*VP*). In addition to FS, mitochondria contain *FM* (NHHS Fe^{II}) and *MP* (mitochondrial nanoparticles). Other non-iron species include O_2 and *ROS* in the mitochondrial matrix. Mass balance of iron requires that

$$[Fe]_{cell} = f_{cyt}[C] + f_{vac}\{[F2] + [F3] + [VP]\} + f_{mit}\{[FM] + [FS] + [MP]\} \quad \text{(Eq. 2)}$$

where f_{vac}, f_{mit}, and f_{cyt} are fractional volume ratios (volume of the designated compartment divided by the volume of the cell). The ordinary differential equations that define the Dual-Reg variant of the model are given by the following equations.

$$\frac{d[C]}{dt} = \frac{R_{cyt}[N]}{K_{cyt} + [N]}Reg_{-C} \cdot Reg_{-FS} - \frac{V_{mit}}{V_{cyt}}\frac{R_{mit}[C]}{K_{mit} + [C]}Reg_{-C} \cdot Reg_{-FS} - \frac{V_{vac}}{V_{cyt}}\frac{R_{vac}[C]}{K_{vac} + [C]}Reg_{+C} \cdot Reg_{+FS} - \alpha[C] \quad \text{(Eq. 3)}$$

$$\frac{d[FM]}{dt} = \frac{R_{mit}[C]}{K_{mit} + [C]}Reg_{-C} \cdot Reg_{-FS} - \frac{R_{isu}[FM]}{K_{isu} + [FM]} - k_{mp}[FM][O2] - \alpha[FM] \quad \text{(Eq. 4)}$$

$$\frac{d[F2]}{dt} = \frac{R_{vac}[C]}{K_{vac} + [C]}Reg_{+C} \cdot Reg_{+FS} - k_{23}\ [F2] \cdot Reg_{+C} \cdot Reg_{+FS} - \alpha[F2] \quad \text{(Eq. 5)}$$

$$\frac{d[FS]}{dt} = \frac{R_{isu}[FM]}{K_{isu} + [FM]} - \alpha[FS] \quad \text{(Eq. 6)}$$

$$\frac{d[MP]}{dt} = k_{mp}[FM][O2] - \alpha[MP] \quad \text{(Eq. 7)}$$

$$\frac{d[F3]}{dt} = k_{23}[F2] \cdot Reg_{+C} \cdot Reg_{+FS} - k_{vp}[F3] - \alpha[F3] \quad \text{(Eq. 8)}$$

$$\frac{d[VP]}{dt} = k_{vp}[F3] - \alpha[VP] \quad \text{(Eq. 9)}$$

$$\frac{d[O2]}{dt} = k_{o2}([RO2] - [O2]) - k_{mp}[FM][O2] - \frac{k_{res}[FS][O2]}{K_{res} + [O2]} \quad \text{(Eq. 10)}$$

$$\frac{d[ROS]}{dt} = k_{mp}[FM][O2] - \alpha[ROS] \quad \text{(Eq. 11)}$$

Ordinary differential equations for the C-Reg and FS-Reg variants were identical except that they lacked FS-sensed and C-sensed *Reg* functions, respectively. The model included 30 floating and 9 fixed parameters (Table 1 and supplemental Table S3). The exponential growth rate for cells that were transitioning smoothly from healthy to diseased state, for any point *i* along that transition, was calculated by solving

$$\frac{[FS]_{health} - [FS]_{previous}}{[FS]_{health} - [FS]_{disease}} = \frac{\alpha_{health} - \alpha_{current}}{\alpha_{health} - \alpha_{disease}} \quad \text{(Eq. 12)}$$

for $\alpha_{current}$ using the FS concentration from the previous point in the transition. Connecting growth rate to [FS] makes sense because FS represents mitochondrial respiratory complexes and hemes. These complexes control cellular energy and perhaps growth rate.

The overall change in cellular iron is given by the following equation (see supplemental information for derivation).

$$\frac{d[Fe_{cell}]}{dt} = f_{cyt}\frac{R_{cyt} \cdot [N]}{K_{cyt} + [N]}Reg_{-C} \cdot Reg_{-FS} - \alpha \cdot [Fe_{cell}] \quad \text{(Eq. 13)}$$

The iron importers that contribute to the import rate R_{cyt} were viewed as a single collective Michaelis-Menten enzyme acting on substrate *N*. For cells in an expanding steady state,

$$[Fe_{cell}] = \frac{f_{cyt}}{\alpha}\frac{R_{cyt} \cdot [N]}{K_{cyt} + [N]}Reg_{-C} \cdot Reg_{-FS} \quad \text{(Eq. 14)}$$

For R_{cyt}, f_{cyt}, *N*, α, K_{cyt}, Reg_{-C}, and Reg_{-FS} values of 410 μM/h, 0.65, 40 μM, 0.2 h^{-1}, 14 μM (Table 1), 1, and 0.4, respectively, the concentration of cellular iron would be ~400 μM.

Oxygen plays a major role in the ISC mutant phenotype, but how it acts on the molecular level remains uncertain. We hypothesize that the matrix of healthy mitochondria is nearly anaerobic and that $[O_2]$ in the matrix is higher in ISC mutants. Because of the activity of cytochrome *c* oxidase on the inner membrane, the concentration of O_2 in the matrix of healthy mitochondria must be lower than in the cytosol (38). However, the magnitude of this difference is uncertain, and $[O_2]$ in the matrix has not been measured. ISC assembly assays require anaerobic conditions (39), as do a number of enzymes in the matrix, including aconitase (40), biotin synthase (41), and lipoic acid synthase (42), supporting our hypothesis.

Our model implies that anaerobic conditions arise in healthy mitochondria because most of the O_2 that diffuses across the IM is rapidly reduced by the respiratory complexes. ISC mutants contain fewer functional respiratory complexes such that more O_2 diffuses into the matrix. Once in the matrix, O_2 reacts with a pool of NHHS Fe^{II} (FM) that is used as feedstock for ISC biosynthesis (8, 43). Reaction of O_2 with FM not only

depletes a reagent needed for ISC biosynthesis; it also generates nanoparticles and ROS. The O_2-dependent loss of FM reduces [FS] further, which causes more O_2 to penetrate the mitochondrial inner membrane. A "disease spiral" results, transforming healthy mitochondria into the ISC mutant diseased state. All of these events are choreographed by our model. This disease spiral would occur regardless of the particular role served by the deleted protein in ISC biosynthesis; the only requirement is that loss of the protein leads to a decline in ISC activity. This situation is indeed observed in that the losses of various proteins, each with different functions in ISC biosynthesis, exhibit the same iron accumulation phenotype.

Ordinary differential Equations 3–11 were coded into Mathematica 9 (Wolfram, Champaign, IL) and numerically integrated using the NDSolve routine and the parameters listed in Table 1. The large number of parameters precluded a rigorously systematic optimization of parameter space. Moreover, the data used in fitting (supplemental Tables S1 and S2) were sparse and had large uncertainties. Thus, parameters were initially adjusted at will to achieve the following desired qualitative behavior. Because [N] increased from iron-deficient conditions, we wanted [C] to increase modestly, [FS] and [FM] to increase quickly and then plateau, vacuolar iron to increase once [N] reached iron-sufficient levels, and [F2] to increase initially and then be replaced by F3 whose concentration would increase sharply at higher [N]. We wanted mitochondrial and vacuolar nanoparticles, and mitochondrial ROS and O_2 to remain at low concentrations throughout the entire range of [N]. In the ISC mutant state (created by lowering R_{isu}), we wanted [MP] to increase dramatically, vacuolar iron to empty, and [C] to remain relatively invariant. Considerable efforts were made to achieve this group of behaviors for each variant.

We then optimized parameters of the Dual-Reg variant by minimizing the following function,

$$\mathrm{RMSD} = \frac{1}{205}\left(\sum_{\text{i=18 Table S2 entries}} wf_i \sum_{\text{j=FM,FS,MP,F3,VP,Fe}^{II}} \frac{|[S]_{i,j} - [D]_{i,j}|}{[\mathrm{Fe}]_{\mathrm{cell},i}} + \sum_{\text{m=43 Table S1 entries}} \frac{2|[S]_m - [D]_m|}{[S]_m + [D]_m} \right) \quad \text{(Eq. 15)}$$

where $[S]_{i,j}$ and $[D]_{i,j}$ are the simulated and experimental concentrations, respectively, for six components (j = *F3*, *VP*, *FM*, *FS*, *MP*, and *NHHS*, Fe^{II}) measured for experiments i = 1–18 involving WT, ISC mutant, ΔCCC1, and CCC1-UP fermenting cells (supplemental Table S2). Weighting factors wf_i equaled 1 for each experiment except for that involving an ISC mutant. In this case, wf_i equaled 10 so as to emphasize the ISC phenotype relative to other experiments. $[\mathrm{Fe}]_{\mathrm{cell},i}$ is the whole-cell iron concentration for experiment i. The second term refers to the 43 comparisons listed in supplemental Table S1. Overall, there were 151 comparisons between experiment and simulation, with six comparisons weighted by 10 (205 comparisons with these weights included).

For fitting, each modeling parameter was increased and decreased while all others were held fixed. The minimum RMSD obtained was called RMSD_{min}. Optimized simulation values are given in Table 1. To evaluate sensitivities, RMSDs obtained when a given parameter was 10% greater (RMSD_+) and 10% lesser (RMSD_-) than its optimal value were averaged and divided by RMSD_{min} (supplemental Table S3). Once the Dual-Reg variant was optimized, the C-reg and FS-reg versions were generated by removing the appropriate Reg functions.

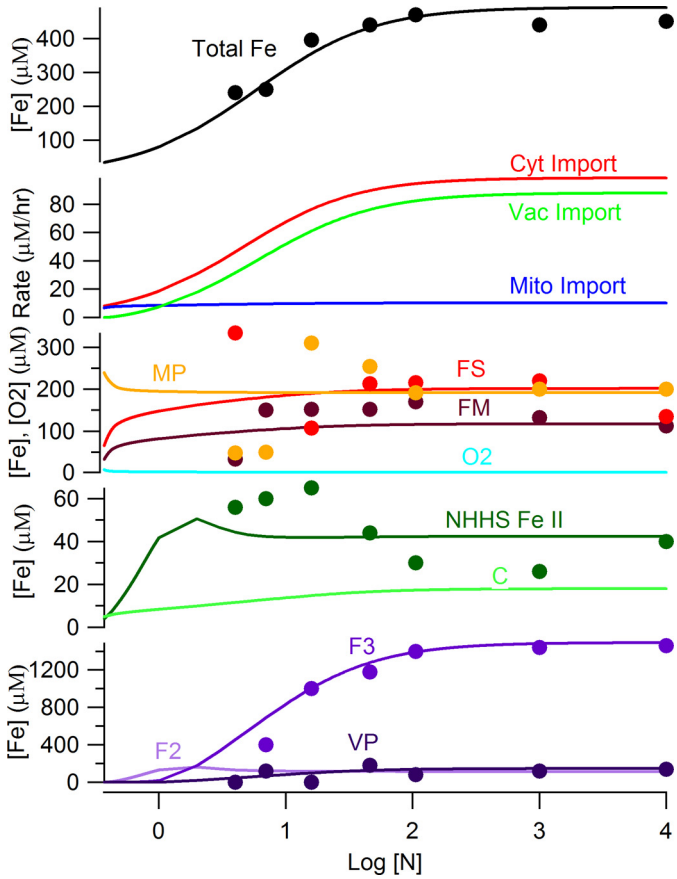

FIGURE 3. **Simulated concentrations of iron components in *S. cerevisiae* at increasing concentrations of iron in the growth medium.** The Dual-Reg variant was assumed. The trace of [C] has been multiplied by 5 for ease of viewing.

Results

The optimized Dual-Reg variant simulated iron import and trafficking in exponentially growing fermenting WT cells with relatively high fidelity; RMSD_{min} was 0.33, nearly half of that obtained using the FS-Reg variant (RMSD_{min} = 0.54) and four times less than obtained using the C-Reg variant (RMSD_{min} = 1.3). The total iron concentration in simulated cells ranged from ~60 μM at [N] = 0.37 μM to ~450 μM at [N] > 100 μM. This is similar to iron concentrations in real cells. The rate of iron import into mitochondria was nearly constant over the entire range of [N], and at low [N] this rate dominated cellular iron traffic flow (Fig. 3). Vacuoles were largely devoid of iron at [N] < 1 μM, but they were half-filled at [N] = ~10 μM and completely filled by [N] = ~40 μM. At [N] > 5 μM, the flow of iron into vacuoles exceeded that into mitochondria.

The simulated concentrations of mitochondrial iron species FM and MP were relatively invariant over the considered range

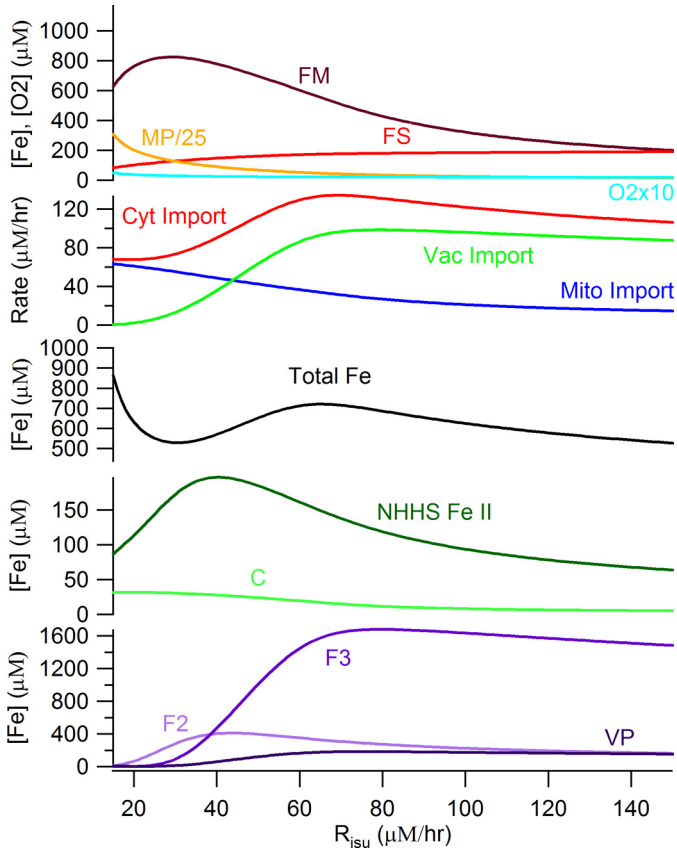

FIGURE 4. **Simulated concentrations of iron components in *S. cerevisiae* at increasing rates by which iron-sulfur clusters and heme centers are synthesized.** The Dual-Reg model variant is assumed along with [N] = 40 μM. The diseased state is on the *left*; the healthy state is on the *right*.

of [N]; [FS] was similarly invariant except for a decline at low [N]. At [N] > 10 μM, the concentrations of all three mitochondrial iron-containing species plateaued near the means of highly scattered experimental values. In simulated healthy cells, mitochondrial O_2 and ROS levels were near 0 throughout the range of [N] (not shown). Simulated vacuolar iron levels were near to experimental values over all [N] (Fig. 3). At low [N], F2 dominated vacuolar iron, but most of this oxidized to F3 at [N] > ~5 μM. [VP] was near 0 at low [N], but it gradually increased as [N] increased. Simulated concentrations of C increased from 2.3 to 3.5 μM as [N] increased from ~0.37 to 30 μM. At higher [N], [C] plateaued at ~3.5 μM. We regard this as well regulated, in that an 80-fold change of [N] resulted in a ~1 μM change in [C]. The collective NHHS Fe^{II} species (0.65[C] + 0.1[FM] + 0.25[F2]) increased to ~50 μM near [N] = 5 μM (mostly because of the accumulation of F2). At higher [N], these species collectively declined to ~40 μM (mainly because of a shift from F2 to F3). This behavior is similar to what is observed experimentally.

To simulate the ISC phenotype, we incrementally reduced the rate of ISC synthesis (R_{isu}) from 250 μM/h, the rate for healthy cells, to 15 μM/h. The concentration plots of all species changed significantly at 30 < R_{isu} < 100 μM/h (Fig. 4). In this regime [FS] declined and [FM] increased more dramatically than at higher R_{isu} rates. These changes are easily rationalized, because R_{isu} is the rate by which FM converts to FS. Other observed changes are secondary effects caused by shifts in regulation due to declining [FS]. These include a decline in vacuolar iron levels and increases in the rates of iron import into the cytosol and into mitochondria.

At R_{isu} < 30 μM/h, even more dramatic changes occurred, all associated with the ISC disease spiral. The primary event causing these changes was a decline of [FS] to concentrations below those required to maintain the matrix in an anaerobic state. The O_2 that penetrates the matrix under these conditions reacts with FM, causing its decline, as well as an increase in ROS and MP concentrations. The loss of FM slows the rate of FS production further, leading to the spiraling effect. The decline in [FS] also causes cytosolic and mitochondrial import valves to open (and the vacuolar iron import valve to close) such that iron rushes into the cytosol, out of the vacuole and into mitochondria where it accumulates as MP. Some FM is not consumed in the ISC diseased state, such that the steady state ratio of [FM]/[Fe_{mit}] is ~7%. This is similar to the Mössbauer spectral intensity of mitochondria isolated from ISC mutant cells, which exhibit features of NHHS Fe^{II} in addition to the dominating nanoparticles (21, 22). The origin of this NHHS Fe^{II} as an expanded FM pool had been unexplained prior to this model.

The disease spiral is delayed and moderated under microerophilic conditions (RO2 = 1 μM) (Fig. 5*A*). When the system lacks O_2, FM cannot convert into nanoparticles, and [FS] only declines marginally. At R_{isu} < 40 μM/h, low [FS] and an assumed low growth rate result in higher iron levels in the cell and mitochondria, such that [FM] increases dramatically, reaching 6 mM at R_{isu} = 20 μM/h. Thus, the model predicts that the iron content of mitochondria isolated from ISC mutant cells grown under anaerobic condions will be dominated by NHHS Fe^{II} rather than by nanoparticles. We are examining this prediction experimentally.

Most component traces of the C-Reg variant were similar to those of the Dual-Reg variant, but vacuolar iron in the C-Reg variant did not empty as [FS] declined in simulating the ISC mutant state (Fig. 5*B*). Cellular iron in C-Reg cells increased largely because the growth rate declined, and vacuoles imported that iron because they could not sense the decline of [FS] in mitochondria. There was also no increase in the rate of iron import into mitochondria during formation of the ISC diseased state (Fig. 5*C*), in contrast to what is observed.

The FS-Reg variant exhibited acceptable behavior overall except that [C] increased to exceedingly high (mM) levels under ISC mutant conditions (Fig. 5*B*). Such unrealistically high concentrations arise because there is no Reg_{-C} valve to curtail the flow of iron in slowly growing cells in which the Reg_{-FS} valve is fully opened.

We next examined the ability of the Dual-Reg variant to reproduce the phenotype of nine genetic strains including ΔYFH1, ΔMRS3/4, Mrs3/4 overexpression, ΔCCC1, CCC1 overexpression, Aft1/2–1^{UP}, ΔYFH1:ΔMRS3/4, ΔYFH1:MRS3/4 overexpression, and ΔCCC1:ΔMRS3/4 (supplemental Tables S1 and S2). We simulated each strain by only adjusting the rate(s) in our model that was(were) associated with the particular genetic modification. Rates for deletion strains were not assigned exactly to 0 because the cells contain secondary pathways that remain operational despite the deletion. The model

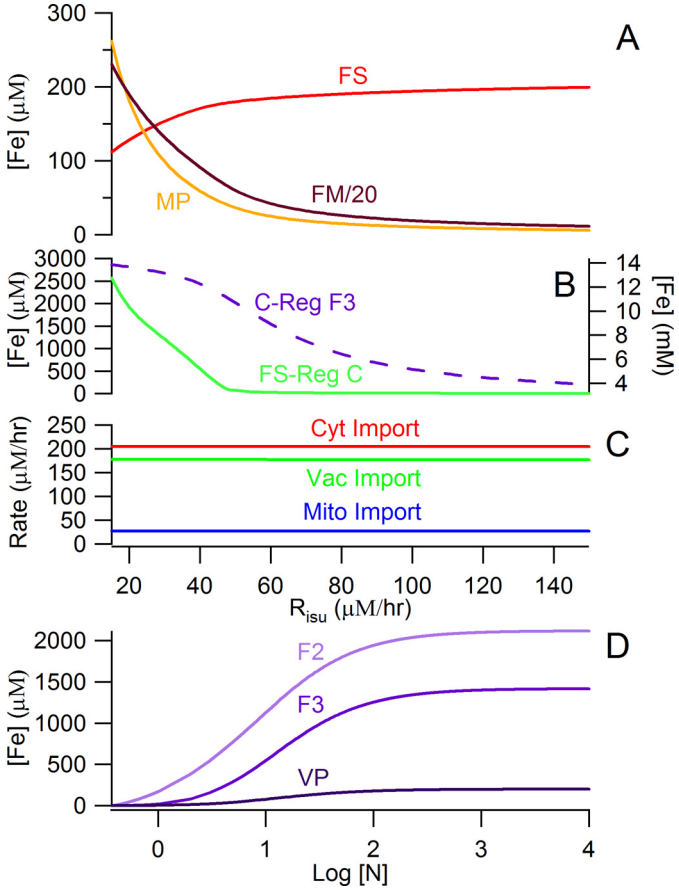

FIGURE 5. **Selected plots from simulations.** *A*, concentrations of mitochondrial iron species under anaerobic growth conditions assuming the Dual-Reg variant. In the diseased state, [FM] is ~20-fold higher than [MP]. *B*, [F3] (*dashed purple line*, *right axis*) simulated by the C-Reg variant does not decline in the diseased state. [C] (*green line*, *left axis*) simulated by the FS-Reg variant increases to unrealistically high concentrations in the diseased state. *C*, import rates simulated by the C-Reg variant are invarient in the diseased state: no accumulation of iron in mitochondria. *D*, simulation of [F2] and [F3] by the Dual-Reg variant in CCC1-UP cells that are adenine-deficient. [F2] is subtantially higher than [F3] as observed.

implicitly includes all pathways of iron into the cytosol, into mitochondria and vacuoles, whereas the genetic strains perturb only a particular pathway.

The most unusual simulated behavior was that of CCC1-UP, which showed high [F2] and low [F3] under conditions where the WT strain is dominated by F3 (Fig. 5*D*). This shift was due to a down-regulation of k_{23} in the simulated CCC1-UP strain, attributed to a more reducing vacuolar environment. In ~65% of all literature cases reported in supplemental Table S1, model simulations "trended" in the observed direction and had reasonable quantitative agreement. Model simulations fitted even better to the Mössbauer-based data of supplemental Table S2. This overall ability to reproduce observed behaviors from the literature and from previous studies in our lab, although not uniformly successful, suggests that many aspects of this simple model are correct.

Finally, we evaluated the sensitivity of model parameters (supplemental Table S3). The rate of iron import into mitochondria was the most sensitive parameter, followed by rate constants for O_2 reacting with FM, for respiration and for nanoparticle formation. The rate of ISC/heme biosynthesis was also sensitive. The model was sensitive to the set point concentrations of FS and to Michaelis-Menten K_m terms involving the import of cytosolic iron into mitochondria, the conversion of FM into FS, and the reduction of O_2 in respiration.

The optimized setpoint concentration for FS, averaged for all four sites, was 170 ± 30 μM. This was comparable to the average concentrations of FS in mitochondria (~200 μM), and it suggests that the FS-Reg valves were opening and closing as designed. The average *sen* factor for FS-Reg functions was 8 ± 2, indicating the need for sensitive regulation.

In contrast, the model was relatively insensitive to parameters associated with C regulation. Set point concentrations for C were highly variable, including values of 27, 80, 1.2, and 2 μM for cytosolic iron import, mitochondrial iron import, vacuolar iron import, and vacuolar Fe^{II} oxidation, respectively. Those for cytosolic and mitochondrial iron import differed from the simulated range of C concentrations (2–4 μM). This means that under most circumstances, the C-Reg valves "controlling" import into the cytosol and mitochondria were fully opened such that these import rates were essentially controlled only by [FS]. C-regulation played a stronger role in vacuolar iron import and oxidation, especially with variations in [N].

Discussion

Immediately following the discovery of Aft1-dependent regulation in 1995, cytosolic iron was commonly assumed to be the sensor of a classic homeostatic regulatory system for controlling iron import and trafficking in yeast cells. This assumption was based on the response of healthy WT cells to changes in the iron concentration of the growth medium. Starting in the early 2000s, cellular iron overload caused by defects in mitochondrial ISC activity revealed the importance of this activity in cellular iron regulation. The classic model predicted that the massive import of iron into ISC-defective mitochondria resulted from an iron-deficient cytosol, which stimulated iron import by activating the iron regulon. Unexpectedly, evidence suggested that the cytosol in ISC mutant cells is iron-replete.

Once it was established that events in the mitochondria impacted those in the nucleus, focus shifted to how such information was transferred from mitochondria to nucleus. In the last decade, many details regarding this mitochondrial → nuclear signal transduction pathway have been established.

Included in this intellectual journey was the conclusion that cytosolic iron is NOT sensed in regulation. However, our study suggests that both cytosolic iron and mitochondrial ISC activity are sensed. Fe_{cyt}-sensing plays an important regulatory role when healthy cells are grown in iron-deficient, iron-sufficient, and iron excess medium (especially with regard to vacuolar iron import and oxidation). In these cases, the level of ISC assembly is relatively constant, such that the rates of iron import into the cytosol and mitochondria are largely invariant. This leads to the observed relative invariance of iron content in mitochondria. On the other hand, when mitochondrial ISC activity is attenuated or halted, FS-based regulation controls these iron import rates.

Both Fe_{cyt} and mitochondrial ISC activity could be regulatory sensors if both were required to generate a single downstream

signal for the mitochondrial-nuclear signal transduction pathway. This requirement would be fulfilled if Fe_{cyt} reacted in the cytosol with X-S that had been exported from the mitochondria to generate the Fe_2S_2 cluster in the $Grx{\cdot}Fe_2S_{2c}Grx$ homodimer (see red star in Fig. 2). When Fe_{cyt} is limiting and X-S abundant, $[Grx{\cdot}Fe_2S_2{\cdot}Grx]$ would be limited, which would activate the iron regulon. In this circumstance, Fe_{cyt} would play the dominant regulatory role. On the other hand, when X-S is limiting and Fe_{cyt} is abundant, $[Grx{\cdot}Fe_2S_2{\cdot}Grx]$ would also be limiting, and the iron regulon would again be activated. However, [X-S] would play the dominant regulatory role. It is only when Fe_{cyt} AND X-S are both abundant (relative to the amount of Grx available) that the iron regulon would not be activated. This is the situation found in healthy WT cells grown on iron-sufficient (or iron excess) conditions. These considerations were assumed in deriving the product function used in the Dual-Reg variant.

Remarkably, dual regulation was proposed in 2003 by Mühlenhoff *et al.* (10) based on their perceptive observation that both deletion and overexpression of Mrs3/4 activated the iron regulon. They posited that deleting Mrs3/4 caused low levels of ISC biosynthesis (thereby stimulating the iron regulon), whereas overexpressing Mrs3/4 caused low levels of Fe_{cyt} (also stimulating the iron regulon). Kaplan and co-workers (11, 12, 36) also interpreted particular experiments assuming that both cytosolic iron and ISC activity regulate iron traffic in yeast.

ISC biosynthesis activity might regulate iron trafficking to help mitochondria import more iron when cells transition from fermentation to respiration. In the late 1980s, Raguzzi, Lesuisse, and Crichton (44) hypothesized that vacuolar iron is mobilized during this metabolic transition. Respiring cells contain approximately three times the concentration of mitochondria as fermenting cells, indicating that the metabolic shift involves mitochondriogenesis (45). Some of the iron for this process comes from mobilized vacuolar iron. The trigger for mitochondriogenesis (perhaps low glucose levels) may not be perfectly coordinated to an increase in the rate of iron import into mitochondria. In this case, growing and dividing mitochondria might experience a transitory period in which insufficient ISCs are made. This might be sensed by a lower than set point concentration of X-S in the cytosol, which might stimulate the ISC mutant phenotype (importing more iron into the cell, exporting vacuolar iron into the cytosol, and importing more Fe_{cyt} into mitochondria). The essential difference is that in healthy respiring cells, the imported iron *can* be used to make ISCs, whereas in ISC mutant cells, it cannot. Accordingly, the up-regulation of iron import, which generates nanoparticle iron in ISC mutant cells, is "earmarked" for ISC biosynthesis in healthy cells. In healthy cells, once sufficient ISCs are made, the signal (X-S) indicating this would attenuate further iron import and allow vacuolar iron stores to be replenished. In contrast, ISC mutant cells cannot use that iron to make ISCs, and so X-S is not made in sufficient amounts to shut down the coordinated import of iron into mitochondria; thus, vacuoles remain devoid of iron, whereas excessive iron pours into mitochondria, generating large amounts of nanoparticles and ROS as it reacts with O_2. This leads to the iron accumulation phenotype that defines ISC-associated diseases.

Mathematical models of biochemical processes in cells become increasingly insightful as the complexity of such processes and the amount of relevant information increases. Such models have the unique ability to integrate the pieces of the puzzle and allow the entire process to be viewed from a systems' level perspective. Modeling the progression from healthy to diseased states is a powerful way to understand the mechanism of diseases and to evaluate the efficacy of different treatments. We hope that further developments of this model will clarify the complex chemical relationships that collectively cause Friedreich's ataxia and other iron accumulation diseases and that such models might promote more effective treatments.

Author Contributions—J. D. W. helped develop the model, wrote the software code, and executed all simulations. P. A. L. designed the model, provided advice, and wrote most of the paper. Both authors reviewed and approved the final version of the manuscript.

Acknowledgment—We thank Dr. Zhigang Zhang for advice in designing the model.

References

1. Outten, C. E., and Albetel, A. N. (2013) Iron sensing and regulation in *Saccharomyces cerevisiae*: ironing out the mechanistic details. *Curr. Opin. Microbiol.* **16,** 662–668
2. Kosman, D. J. (2013) Iron metabolism in aerobes: managing ferric iron hydrolysis and ferrous iron autoxidation. *Coord. Chem. Rev.* **257,** 210–217
3. Chen, O. S., Crisp, R. J., Valachovic, M., Bard, M., Winge, D. R., and Kaplan, J. (2004) Transcription of the yeast iron regulon does not respond directly to iron but rather to iron-sulfur cluster biosynthesis. *J. Biol. Chem.* **279,** 29513–29518
4. Li, L., Miao, R., Bertram, S., Jia, X., Ward, D. M., and Kaplan, J. (2012) A role for iron-sulfur clusters in the regulation of transcription factor yap5-dependent high iron transcriptional responses in yeast. *J. Biol. Chem.* **287,** 35709–35721
5. Holmes-Hampton, G. P., Jhurry, N. D., McCormick, S. P., and Lindahl, P. A. (2013) Iron content of *Saccharomyces cerevisiae* cells grown under iron-deficient and iron-overload conditions. *Biochemistry* **52,** 105–114
6. Cockrell, A., McCormick, S. P., Moore, M. J., Chakrabarti, M., and Lindahl, P. A. (2014) Mössbauer, EPR, and modeling study of iron trafficking and regulation in ΔCCC1 and Ccc1p-up *Saccharomyces cerevisiae*. *Biochemistry* **53,** 2926–2940
7. Park, J., McCormick, S. P., Cockrell, A. L., Chakrabarti, M., and Lindahl, P. A. (2014) High-spin ferric ions in *Saccharomyces cerevisiae* vacuoles are reduced to the ferrous state during adenine-precursor detoxification. *Biochemistry* **53,** 3940–3951
8. Holmes-Hampton, G. P., Miao, R., Garber Morales, J., Guo, Y., Münck, E., and Lindahl, P. A. (2010) A nonheme high-spin ferrous pool in mitochondria isolated from fermenting *Saccharomyces cerevisiae*. *Biochemistry* **49,** 4227–4234
9. Foury, F., and Roganti, T. (2002) Deletion of the mitochondrial carrier genes MRS3 and MRS4 suppresses mitochondrial iron accumulation in a yeast frataxin-deficient strain. *J. Biol. Chem.* **277,** 24475–24483
10. Mühlenhoff, U., Stadler, J. A., Richhardt, N., Seubert, A., Eickhorst, T., Schweyen, R. J., Lill, R., and Wiesenberger, G. (2003) A specific role of the yeast mitochondrial carriers Mrs3/4p in mitochondrial iron acquisition under iron-limiting conditions. *J. Biol. Chem.* **278,** 40612–40620
11. Chen, O. S., and Kaplan, J. (2000) CCC1 suppresses mitochondrial damage in the yeast model of Friedreich's ataxia by limiting mitochondrial iron accumulation. *J. Biol. Chem.* **275,** 7626–7632
12. Li, L., Chen, O. S., McVey Ward, D., and Kaplan, J. (2001) CCC1 is a transporter that mediates vacuolar iron storage in yeast. *J. Biol. Chem.* **276,** 29515–29519
13. Yamaguchi-Iwai, Y., Dancis, A., and Klausner, R. D. (1995) Aft1: a media-

tor of iron-regulated transcriptional control in *Saccharomyces cerevisiae*. *EMBO J.* **14,** 1231–1239
14. Yamaguchi-Iwai, Y., Stearman, R., Dancis, A., and Klausner, R. D. (1996) Iron-regulated DNA binding by the Aft1 protein controls the iron regulon in yeast. *EMBO J.* **15,** 3377–3384
15. Rutherford, J. C., Jaron, S., Ray, E., Brown, P. O., and Winge, D. R. (2001) A second iron-regulatory system in yeast independent of Aft1p. *Proc. Natl. Acad. Sci. U.S.A.* **98,** 14322–14327
16. Rutherford, J. C., Jaron, S., and Winge, D. R. (2003) Aft1p and Aft2p mediate iron-responsive gene expression in yeast through related promoter elements. *J. Biol. Chem.* **278,** 27636–27643
17. Courel, M., Lallet, S., Camadro, J. M., and Blaiseau, P. L. (2005) Direct activation of genes involved in intracellular iron use by the yeast iron-responsive transcription factor Aft2 without its paralog Aft1. *Mol. Cell. Biol.* **25,** 6760–6771
18. Yamaguchi-Iwai, Y., Ueta, R., Fukunaka, A., and Sasaki, R. (2002) Subcellular localization of Aft1 transcription factor responds to iron status in *Saccharomyces cerevisiae*. *J. Biol. Chem.* **277,** 18914–18918
19. Poor, C. B., Wegner, S. V., Li, H., Dlouhy, A. C., Schuermann, J. P., Sanishvili, R., Hinshaw, J. R., Riggs-Gelasco, P. J., Outten, C. E., and He, C. (2014) Molecular mechanism and structure of the *Saccharomyces cerevisiae* iron regulator Aft2. *Proc. Natl. Acad. Sci. U.S.A.* **111,** 4043–4048
20. Babcock, M., de Silva, D., Oaks, R., Davis-Kaplan, S., Jiralerspong, S., Montermini, L., Pandolfo, M., and Kaplan, J. (1997) Regulation of mitochondrial iron accumulation by Yfh1p, a putative homolog of frataxin. *Science* **276,** 1709–1712
21. Miao, R., Martinho, M., Morales, J. G., Kim, H., Ellis, E. A., Lill, R., Hendrich, M. P., Münck, E., and Lindahl, P. A. (2008) EPR and Mössbauer spectroscopy of intact mitochondria isolated from Yah1p-depleted *Saccharomyces cerevisiae*. *Biochemistry* **47,** 9888–9899
22. Miao, R., Kim, H., Koppolu, U. M., Ellis, E. A., Scott, R. A., and Lindahl, P. A. (2009) Biophysical characterization of the iron in mitochondria from Atm1p-depleted *Saccharomyces cerevisiae*. *Biochemistry* **48,** 9556–9568
23. Chen, O. S., Hemenway, S., and Kaplan, J. (2002) Inhibition of Fe-S cluster biosynthesis decreases mitochondrial iron export: evidence that yfh1p affects Fe-S cluster synthesis. *Proc. Natl. Acad. Sci. U.S.A.* **99,** 12321–12326
24. Srinivasan, V., Pierik, A. J., and Lill, R. (2014) Crystal structures of nucleotide-free and glutathione-bound mitochondrial ABC transporter Atm1. *Science* **343,** 1137–1140
25. Lee, J. Y., Yang, J. G., Zhitnitsky, D., Lewinson, O., and Rees, D. C. (2014) Structural basis for heavy metal detoxification by an Atm1-type ABC exporter. *Science* **343,** 1133–1136
26. Schaedler, T. A., Thornton, J. D., Kruse, I., Schwarzländer, M., Meyer, A. J., van Veen, H. W., and Balk, J. (2014) A conserved mitochondrial ATP-binding cassette transporter exports glutathione polysulfide for cytosolic metal cofactor assembly. *J. Biol. Chem.* **289,** 23264–23274
27. Mapolelo, D. T., Zhang, B., Randeniya, S., Albetel, A. N., Li, H., Couturier, J., Outten, C. E., Rouhier, N., and Johnson, M. K. (2013) Monothiol glutaredoxins and A-type proteins: partners in Fe-S cluster trafficking. *Dalton Transactions* **42,** 3107–3115
28. Ojeda, L., Keller, G., Mühlenhoff, U., Rutherford, J. C., Lill, R., and Winge, D. R. (2006) Role of glutaredoxin-3 and glutaredoxin-4 in the iron regulation of the Aft1 transcriptional activator in *Saccharomyces cerevisiae*. *J. Biol. Chem.* **281,** 17661–17669
29. Li, H., Mapolelo, D. T., Dingra, N. N., Naik, S. G., Lees, N. S., Hoffman, B. M., Riggs-Gelasco, P. J., Huynh, B. H., Johnson, M. K., and Outten, C. E. (2009) The yeast iron regulatory proteins Grx3/4 and Fra2 form heterodimeric complexes containing a [2Fe-2S] cluster with cysteinyl and histidyl ligation. *Biochemistry* **48,** 9569–9581
30. Li, L., Jia, X., Ward, D. M., and Kaplan, J. (2011) Yap5 protein-regulated transcription of the TYW1 gene protects yeast from high iron toxicity. *J. Biol. Chem.* **286,** 38488–38497
31. Li, L., Bagley, D., Ward, D. M., and Kaplan, J. (2008) Yap5 is an iron-responsive transcriptional activator that regulates vacuolar iron storage in yeast. *Mol. Cell. Biol.* **28,** 1326–1337
32. Rietzschel, N., Pierik, A. J., Bill, E., Lill, R., and Mühlenhoff, U. (2015) The basic leucine zipper stress response regulator Yap5 senses high-iron conditions by coordination of [2Fe-2S] clusters. *Mol. Cell Biol.* **35,** 370–378
33. Urbanowski, J. L., and Piper, R. C. (1999) The iron transporter fth1p forms a complex with Fet5 iron oxidase and resides on the vacuolar membrane. *J. Biol. Chem.* **274,** 38061–38070
34. Pedro-Segura, E., Vergara, S. V., Rodríguez-Navarro, S., Parker, R., Thiele, D. J., and Puig, S. (2008) The Cth2 ARE-binding protein recruits the Dhh1 helicase to promote the decay of succinate dehydrogenase SDH4 mRNA in response to iron deficiency. *J. Biol. Chem.* **283,** 28527–28535
35. Robinson, A. J., and Kunji, E. R. (2006) Mitochondrial carriers in the cytoplasmic state have a common substrate binding site. *Proc. Natl. Acad. Sci. U.S.A.* **103,** 2617–2622
36. Li, L., and Kaplan, J. (2004) A mitochondrial-vacuolar signaling pathway in yeast that affects iron and copper metabolism. *J. Biol. Chem.* **279,** 33653–33661
37. Park, J., McCormick, S. P., Chakrabarti, M., and Lindahl, P. A. (2013) The lack of synchronization between iron uptake and cell growth leads to iron overload in *Saccharomyces cerevisiae* during post-exponential growth modes. *Biochemistry* **52,** 9413–9425
38. Koyama, T., Kinjo, M., and Araiso, T. (1989) Oxygen diffusion through mitochondrial membranes. In *Oxygen Transport to Tissue XI* (Rakusan, K., ed) pp. 763–767, Plenum Press, New York
39. Lill, R., and Mühlenhoff, U. (2006) Iron-sulfur protein biogenesis in eukaryotes: components and mechanisms. *Annu. Rev. Cell Dev. Biol.* **22,** 457–486
40. Brown, N. M., Kennedy, M. C., Antholine, W. E., Eisenstein, R. S., and Walden, W. E. (2002) Detection of a [3Fe-4S] cluster intermediate of cytosolic aconitase in yeast expressing iron regulatory protein 1: insights into the mechanism of Fe-S cluster cycling. *J. Biol. Chem.* **277,** 7246–7254
41. Cosper, M. M., Jameson, G. N., Eidsness, M. K., Huynh, B. H., and Johnson, M. K. (2002) Recombinant *Escherichia coli* biotin synthase is a $[2Fe\text{-}2S]^{2+}$ protein in whole cells. *FEBS Lett.* **529,** 332–336
42. Kriek, M., Peters, L., Takahashi, Y., and Roach, P. L. (2003) Effect of iron-sulfur cluster assembly proteins on the expression of *Escherichia coli* lipoic acid synthase. *Protein Expr. Purif.* **28,** 241–245
43. Pandey, A., Pain, J., Ghosh, A. K., Dancis, A., and Pain, D. (2015) Fe-S cluster biogenesis in isolated mammalian mitochondria: coordinated use of persulfide sulfur and iron and requirements for GTP, NADH, and ATP. *J. Biol. Chem.* **290,** 640–657
44. Raguzzi, F., Lesuisse, E., and Crichton, R. R. (1988) Iron storage in *Saccharomyces cerevisiae*. *FEBS Lett.* **231,** 253–258
45. Haurie, V., Boucherie, H., and Sagliocco, F. (2003) The snf1 protein kinase controls the induction of the genes of the iron uptake pathway at the diauxic shift in *Saccharomyces cerevisiae*. *J. Biol. Chem.* **278,** 45391–45396
46. Foster, A. W., Dainty, S. J., Patterson, C. J., Pohl, E., Blackburn, H., Wilson, C., Hess, C. R., Rutherford, J. C., Quaranta, L., Corran, A., and Robinson, N. J. (2014) A chemical potentiator of copper-accumulation used to investigate the iron regulons of *Saccharomyces cerevisiae*. *Mol. Microbiol.* **93,** 317–330